PHYSICAL REVIEW VOLUME 179, NUMBER 5 25 MARCH 1969

Differential Production Cross Sections of Low-Momentum Particles from 12.3-BeV/c Protons on Beryllium and Copper*†

G. J. MARMER,‡ K. REIBEL, D. M. SCHWARTZ, AND A. STEVENS
Ohio State University, Columbus, Ohio 43210

R. WINSTON AND D. WOLFE
The Enrico Fermi Institute, University of Chicago, Chicago, Illinois 60637

C. J. RUSH
Argonne National Laboratory, Argonne, Illinois 60439

P. R. PHILLIPS
Washington University, St. Louis, Missouri 63130

E. C. SWALLOW§
Washington University, St. Louis, Missouri 63130
and
Argonne National Laboratory, Argonne, Illinois 60439

AND

T. A. ROMANOWSKI
Argonne National Laboratory, Argonne, Illinois 60439
and
Ohio State University, Columbus, Ohio 43210

(Received 13 August 1968; revised manuscript received 25 November 1968)

Measurements of the differential production cross sections of pions, kaons, protons, and antiprotons from 12.3-BeV/c protons incident upon copper and beryllium targets were made at the Zero-Gradient Synchrotron at Argonne National Laboratory. These measurements were taken at production angles between 0 and 11.2 deg and covered the momentum range 500–1030 MeV/c. The particles were detected by a time-of-flight technique, supplemented by Čerenkov counters for kaons and antiprotons.

I. INTRODUCTION

THE major purpose of this experiment was the determination of the zero-degree differential production cross sections for kaons, pions, protons, and antiprotons at 500, 820, and 1000 MeV/c from copper and beryllium targets. In addition, at the 1000-MeV/c beam transport settings, deuterons, tritons, and He^{3++} were observed. Finally, data at 5- and 10-deg production angles in the laboratory for short copper and beryllium targets were also collected.[1]

II. EXPERIMENTAL APPARATUS

A. Primary and Secondary Beams

The secondary beam used for this experiment is shown in Fig. 1. To reduce background and multiple scattering, helium bags were installed in the proton beam upstream from the production target and in the secondary beam between the counters S1 and S3A.

The proton beam size (full-width at half-maximum) was measured with radioautographs and found to be 1 cm horizontally by 0.5 cm vertically at the focus. The corresponding beam divergences were 0.55 and 1.6 mrad, respectively. The intensity was typically 4×10^{10} protons per pulse.

The targets were all 2.22 cm in diameter, more than twice the beam size. Copper and beryllium targets varying from 1 to 10 cm in length were used for zero-deg production. For nonzero production angles, only short targets, 1–3 cm in length, were used.

To obtain nonzero production angles, the target was moved into the first bending magnet an appropriate

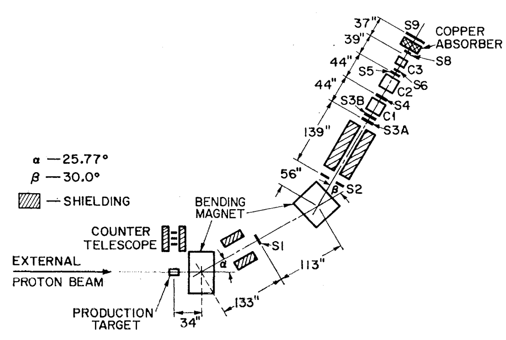

FIG. 1. Secondary particle beam (not to scale). S1–S9 are scintillation counters, C1 and C2 are focusing differential Čerenkov counters, and C3 is a gas threshold Čerenkov counter.

* Work performed under the auspices of the U. S. Atomic Energy Commission.

† Based upon a Ph.D. dissertation submitted by G. J. Marmer to the Ohio State University, 1968.

‡ Present address: Argonne National Laboratory, Argonne, Ill.

§ AMU-ANL Predoctoral Research Fellow.

[1] G. J. Marmer, K. Reibel, D. M. Schwartz, A. Stevens, P. R. Phillips, E. C. Swallow, R. Winston, D. Wolfe, T. A. Romanowski, and C. J. Rush, Argonne National Laboratory Report No. ANL/HEP 6801 (unpublished).

distance and the magnetic field correspondingly altered. Radioautographs of irradiated targets were produced under these conditions to ensure that the proton beam was striking the target as desired.

The solid angle $\Delta\Omega$ and momentum bite $\Delta P/P$ (full-width at half-maximum) accepted by the secondary beam detectors were approximately 6.3×10^{-5} sr and 0.035, respectively. Values of $\Delta\Omega\Delta P$ were computed with the CDC 3600 beam analysis program TRAMP.[2]

B. Proton Beam Monitors

Foil activation was the primary method of monitoring the absolute number of protons incident upon each target. A foil "sandwich" consisting of three 5-mil polyethylene foils followed by two 0.5-mil gold foils was mounted on the upstream end of each target. The α activity of Tb^{149}, produced in the reaction Au^{197}-$(p,15p34n)Tb^{149}$, was counted in a windowless gas-flow-type proportional counter.

The polyethylene foils were used as auxiliary monitors for consistency checks. The β^+ activity of C^{11}, produced in the reaction $C^{12}(p,pn)C^{11}$, was counted in a well counter employing a sodium iodide crystal.

A counter telescope, consisting of three $1\frac{1}{2}$ in.$\times1\frac{1}{2}$ in.$\times\frac{1}{4}$ in. scintillators, viewed the production target at 90° as shown in Fig. 1. A narrow-gap ion chamber was located in the external proton beam, approximately 3 m upstream from the production target. These monitors were used for observing the incident proton intensity as a function of time during each individual run. The correction to the absolute number of incident protons caused by beam-intensity fluctuations was less than 0.5% for the gold-foil measurements and less than 5% for the polyethylene-foil measurements.

C. Secondary Particle Detection

The various types of particles produced were differentiated by time of flight in conjunction with Čerenkov and energy-loss selection techniques. Counter locations are shown in Fig. 1.

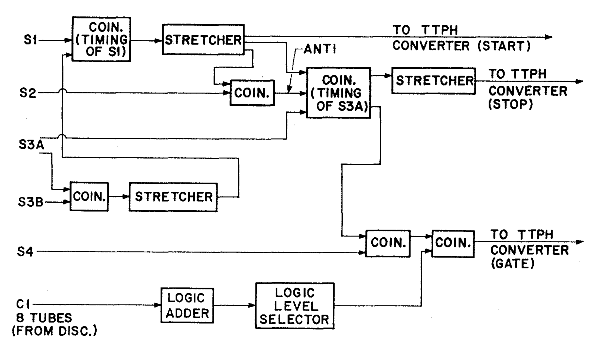

FIG. 2. Simplified schematic drawing showing major electronic components for the kaon logic. The pion and proton logic is identical except for the TTPH gate signal.

[2] G. S. Keyes, TRAMP CDC 3600 version, 1965 (unpublished).

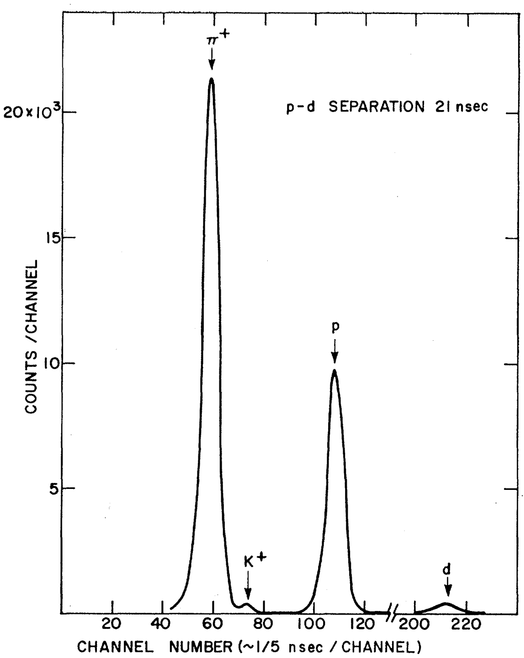

FIG. 3. PHA spectrum at 1000 MeV/c gated by monitor signal.

The first timing counter S1 was a scintillation counter with an air light pipe. S3A, the second timing counter, and S3B were mounted contiguously with their plastic light pipes in opposite directions. S2 was a hole anticoincidence counter as indicated in Fig. 1. A simplified block diagram of the electronic logic is shown in Fig. 2. Two independent time-to-pulse-height converter (TTPH) and pulse-height analyzer (PHA) systems were employed.

1. *Pions and Protons*

The first TTPH system was gated by the signal $M=(S1)(\bar{S2})(S3A)(S3B)$ which signified that a particle had been transported through the system. This spectrum therefore contained pions, kaons, protons, and deuterons (see Fig. 3). The background levels here prohibited accurate determination of the flux of kaons, deuterons, or antiprotons.

2. *Kaons*

The second TTPH and PHA system was utilized to detect kaons and antiprotons. For kaons, the gate signal contained additional information as required from one or both of the eight-tube focusing differential Čerenkov counters[3] C1 and C2. The mode of operation of these counters was dependent upon the secondary beam momentum.

[3] This counter was similar to that discussed by D. A. Hill, D. O. Caldwell, D. H. Frisch, L. S. Osborne, D. M. Ritson, and R. A. Schluter, Rev. Sci. Instr. 32, 111 (1961).

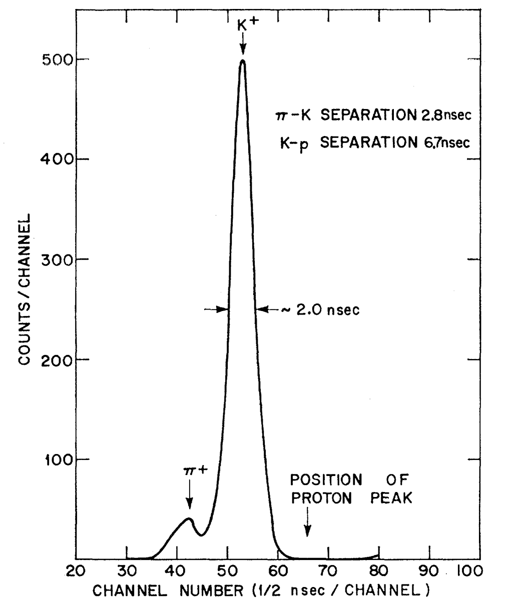

FIG. 4. PHA spectrum at 1000 MeV/c gated by monitor and Čerenkov-counter signals.

At 820 and 1000 MeV/c, glycerol and sugar solution with indices of refraction 1.47 and 1.43, respectively, were used. With these liquids the pion light was trapped in the 2-in.-thick Čerenkov cell, the protons were below threshold, and the kaon light was emitted at the proper angle to be focused onto the photomultiplier tubes. Each Čerenkov counter rejected pions by a factor greater than 30. At 820 MeV/c, the pion and kaon peaks were separated by 4.5 nsec, and one Čerenkov counter (C1) was sufficient to clearly resolve the peaks. At 1000 MeV/c, the separation was slightly less than 3.0 nsec, so both counters were required. A comparison of Figs. 3 and 4 shows the rejection obtained with C1 and C2 in coincidence.

At 500 MeV/c, C1 was used as a threshold counter. C1 detected only pions when filled with water, and this pion signal was then used in anticoincidence to form the desired gate signal. The combination of kaon decay kinematics, and Čerenkov counter geometry prevented more than 3% of the decay products of the kaons from giving a signal.

3. *Antiprotons*

To separate antiprotons at all three moments, C1 was employed as a threshold counter for pions and this signal used in anticoincidence as above. The background was further reduced at 500 MeV/c and 820 MeV/c by reducing the voltage (photomultiplier gain) on S1 and S3B (discrimination by energy loss). Detection efficiencies at reduced voltage were measured with protons in a positive beam.

4. *Heavy Particles*

Deuterons, tritons, and He^{3++} were detected by time of flight with the background again suppressed by reducing the voltage on S1 and S3B.

5. *Electrons and Muons*

The pion signal as described above included electrons and muons, and these beam components were differentiated and subtracted to obtain the true pion flux. The electrons were detected by a threshold Čerenkov counter[4] C3, employing Freon 13 as the radiator. The electron contamination in the beam was deduced from the ratio M(S4)(S5)(S6)(S8)(C3)/M(S4)(S5)(S6)(S8). This ratio was corrected for pion decays in flight to yield the contamination at S3A. A suitable thickness of copper was used to distinguish muons from the pions and electrons.

TABLE I. Typical magnitudes of quantities entering into the yield calculation and their contribution to the final yield uncertainty.

Quantity		Typical value of quantity	Contribution to yield uncertainty
Number of particles	N	10^2–10^6	10–0.1%
PHA dead-time correction	A	1–7	<0.25%
Particle decay correction	D	1.24–34.2	1–6%
Čerenkov counter absorption and scattering correction	C	1.10–1.20	2–8%
Correction for multiple scattering in S1	S	1.01	<1%
Correction for S2 random anticoincidences	R	1.01	<1%
S1, S3 dead-time correction	T	1.0–1.1	<1%
Number of incident protons	N_p	5×10^{12}	1–4%[a]
$\Delta\Omega\Delta p$ [$sr^{-1}(BeV/c)^{-1}$]		10^{-6}–2×10^{-6}	2.5%
S1, S3B high-voltage plateau correction (for antiprotons and heavy particles)	H	1.0–1.25	3%
Electron contamination		15–50%	1–2.5%
Muon contamination		3%	<1%

[a] This does not include the 5% uncertainty in the gold activation cross section, 1.02±0.5 mb.

III. DATA ANALYSIS

A. Yields

The following corrections were applied to the raw data to obtain the particle yield, which is the difference

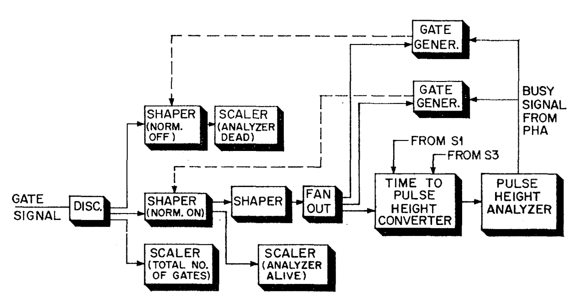

FIG. 5. Simplified schematic drawing showing the paralysis logic for monitoring the PHA dead time.

[4] Jacques Sayag, Compteur Čerenkov à Gaz Pour Electrons, Saclay (unpublished).

between the "target-in" yield and "target-out" yield. In every "target-out" run, a gold and polyethylene foil "sandwich" was installed at the target position.

$$Y_{\text{final}} = Y - Y_{\text{target out}},$$

$$Y = NADCSRTH/N_p\Delta\Omega\Delta P$$
$$= \text{yield [particles/(BeV/}c\text{) sr incident proton]},$$

N is the number of counts under the appropriate time-of-flight peak, A is the pulse-height-analyzer dead-time correction, D is the particle decay correction, C is the Čerenkov counter absorption and scattering correction, S is the correction for multiple scattering losses due to S1, R is the correction for S2 random anticoincidences, T is the dead-time correction for S1, S3A, S3B, N_p is the number of protons incident on the target, $\Delta\Omega\Delta P$ is the product of solid angle and momentum bite of the secondary beam, H is the S1, S3A efficiency correction for reduced high voltage (antiprotons and heavy particles only).

A discussion of the more significant of the above parameters follows. N_p has already been treated in Sec. II B, and the correction for reduced photomultiplier voltage was mentioned in Sec. II C under Antiprotons.

1. *Number of Observed Counts*

The total number of counts observed for a given type of particle in a run was obtained by summing the number of counts in each channel under the time-of-flight peak and subtracting from it the random background in this time region.

2. *Pulse-Height-Analyzer Dead-Time Correction*

The multiplicative correction factor due to PHA dead time (approximately 50 μsec/input) varied from nearly unity for antiprotons to as high as seven for pions and protons from thick copper targets. This dead time was monitored as follows (see Fig. 5). The first pulse which

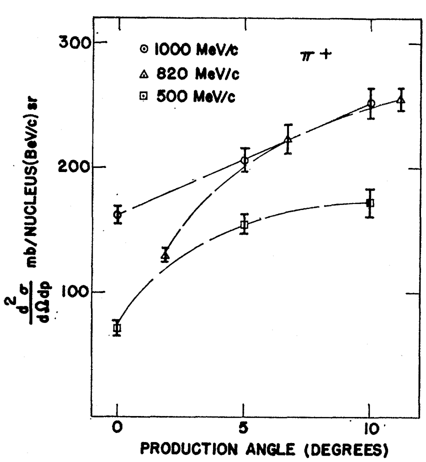

FIG. 6. Differential production cross sections of π^+ from beryllium.

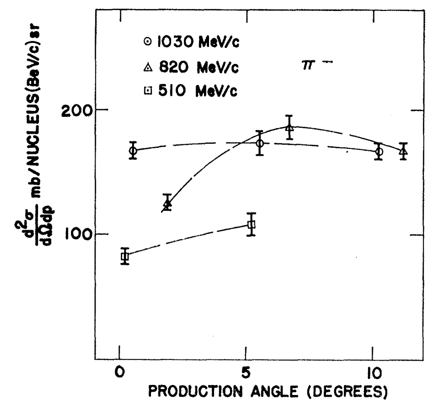

FIG. 7. Differential production cross sections of π^- from beryllium.

gated the TTPH converter also triggered two zero-dead-time gate generators. One of these paralyzed the fast logic to the PHA (normally on) during the entire time required to analyze the output of the time-to-height converter. The other gate generator enabled a fast logic circuit (normally off) to count the number of pulses arriving while the PHA was busy. Thus, the number of counts that were analyzed and the number of counts that arrived while the PHA was busy were both recorded. The sum of these two always agreed (to better than 0.25%) with the total number of gates.

3. *Absorption and Scattering*

Multiple scattering and absorption of particles in the various detectors was measured by observing the decrease in secondaries as additional material was

TABLE II. Differential production cross sections of $\pi^\pm$, $K^\pm$, p, $\bar{p}$ from copper.

Particle	Momentum (MeV/c)	$d^2\sigma(\theta)/d\Omega dp$ [mb/nucleus (BeV/c) sr] 0°	5°	10°
π^+	1000	602±21	827±35	918±50
	820	607±32	974±50	1032±33
	500	585±58	821±56	861±70
K^+	1000	47.6±2.4	50.3±2.0	52.1±3.2
	820	43.0±1.6	69.9±4.4	65.1±2.6
	500	21.0±1.6	23.9±5.0	26.5±4.4
p	1000	486±14	607±23	627±34
	820	487±16	645±29	669±19
	500	459±15	522±28	551±57
π^-	1030	633±21	673±21	613±18
	820	695±38	779±34	786±33
	510	553±66	547±42	567±85
K^-	1030	11.4±1.1	10.8±1.1	10.4±1.0
	820	12.2±0.6	21.1±1.1	16.1±1.1
	510	3.7±0.6	6.7±0.8	
$\bar{p}$	1030	0.13±0.05	0.14±0.05	0.13±0.05
	820	0.050±0.038	0.086±0.057	0.064±0.074
d	1000	52.1±5.0	60.3±3.9	57.4±3.8
t	1000	5.50±0.54	6.61±0.45	6.95±0.48
He^{3++}	2000	1.17±0.13	1.33±0.10	1.37±0.11

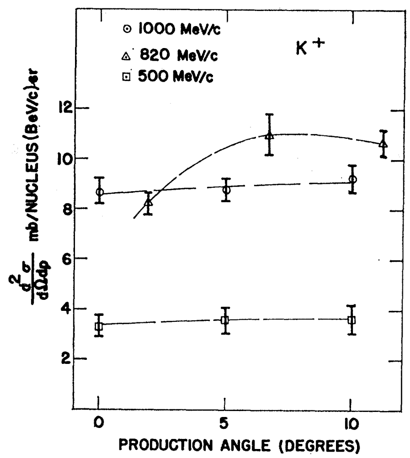

FIG. 8. Differential production cross sections of K^+ from beryllium.

inserted into the beam. Agreement between measured and calculated values was better than 5%.

4. *Errors*

Statistical errors were largest for kaons and antiprotons, particularly at 500 MeV/c. In addition, the random background frequently accounted for 10–20% of the counts under the peak at this low momentum. Although the "pion" peak contained a large number of counts, usually greater than 10^6, anywhere from 10–50% of these were electrons, depending upon target length and material. Typical magnitudes of the quantities entering into the yield calculation and their contribution to the quoted yield errors are listed in Table I.

B. Cross Sections

In order to convert the yield data to differential production cross sections, the following were assumed:

TABLE III. Differential production cross sections of $\pi^\pm$, $K^\pm$, p, $\bar{p}$ from beryllium.

Particle	Momentum (MeV/c)	$d^2\sigma(\theta)/d\Omega dp$ [mb/nucleus (BeV/c) sr] 0°	5°	10°
π^+	1000	162±7	206±9	252±12
	820	130±5	223±12	255±9
	500	71±4	155±8	172±11
K^+	1000	8.66±0.48	8.79±0.46	9.24±0.55
	820	8.28±0.35	11.0±0.8	10.7±0.5
	500	3.30±0.38	3.60±0.51	3.63±0.57
p	1000	65.9±2.4	77.2±2.8	81.3±3.5
	820	61.8±2.0	75.1±3.6	79.2±2.4
	500	46.0±1.8	53.9±2.2	52.2±2.7
π^-	1030	167±7	173±9	167±6
	820	126±5	186±10	167±8
	510	82±6	108±9	
K^-	1030	2.17±0.26	1.95±0.24	2.10±0.23
	820	2.47±0.13	3.55±0.31	3.23±0.25
	510	0.76±0.11	0.99±0.14	
$\bar{p}$	1030	0.038±0.018	0.057±0.032	0.041±0.022
	820	0.009±0.007		
d	1000	1.98 ±0.32	2.64 ±0.38	2.48 ±0.35
t	1000	0.128±0.038	0.184±0.051	0.148±0.041
He^{3++}	2000	0.025±0.009	0.020±0.007	0.017±0.005

(1) The processes of primary protons and secondaries interacting in the target are characterized by exponential absorption with absorption coefficients a and b. (2) Because of ionization energy loss in the target, particles observed with momentum p_0 must be produced at some higher momentum p with appropriately different production cross section. The relation between these cross sections is assumed to take the simple form

$$\sigma_x=\sigma_0[1+f(L-x)],$$

where L is the target length, x is the distance of the production point at which the secondary is produced

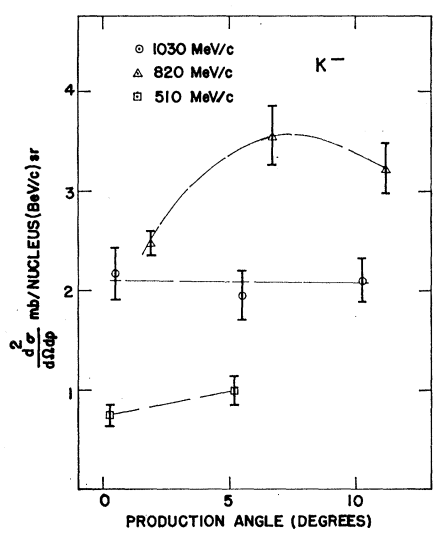

FIG. 9. Differential production cross sections of K^- from beryllium.

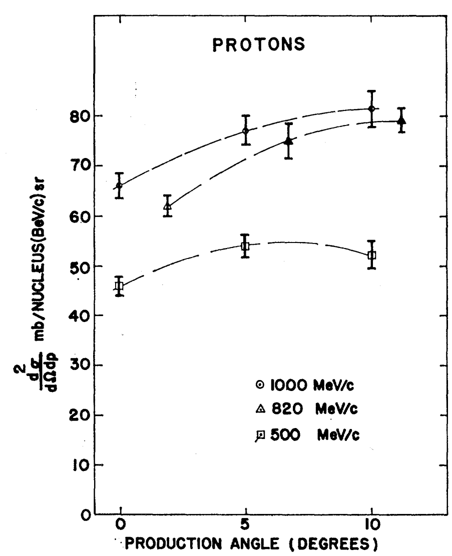

FIG. 10. Differential production cross sections of protons from beryllium.

TABLE IV. Momenta and production angles. Q is the sign of the particle charge; P is the central momentum; ΔP is the momentum acceptance (half-width at half-maximum); θ is the nominal production angle; $(\Delta\theta)_u$ is the uncertainty in θ (half-width); and $(\Delta\theta)_s$ is the approximate angular acceptance about θ (half-width).

Q, P (MeV/c)	ΔP (MeV/c)	θ (deg)	$(\Delta\theta)_u$ (deg)	$(\Delta\theta)_s$ (deg)
+500	9	0.0	0.10	0.64
+500	11	5.0	0.40	0.70
+500	12	10.0	0.40	0.70
−510	9	0.25	0.11	0.64
−510	11	5.2	0.40	0.70
−510	12	10.0	0.40	0.70
±820	13	1.9	0.27	0.64
±820	15	6.7	0.45	0.70
±820	18	11.2	0.43	0.70
+1000	18	0.0	0.10	0.64
+1000	21	5.0	0.40	0.70
+1000	23	10.0	0.40	0.70
−1030	18	0.55	0.11	0.64
−1030	21	5.45	0.40	0.70
−1030	23	10.24	0.40	0.70

from the upstream face of the target, and f is an unknown constant.

Upon integrating over the target length and making suitable approximations and simplifications, one obtains

$$Y(L)=(\rho N_0 L/A)\sigma_0 e^{-(b+a-f)L/2},$$

where $Y(L)$ is the particle yield for target of length L, ρ is the density of target material, A is the atomic weight of the target material, N_0 is Avogadro's number, and $\sigma_0=d^2\sigma/d\Omega dp$ is the differential production cross section.

In this expression there are two unknown parameters, σ_0 and $(b+a-f)$. For each momentum and target material, a set of yields at various target lengths was measured. These data were then fitted to the above functional form by the method of least squares to obtain the two unknown parameters. However, even more information was obtained from the data by observing that $(b+a-f)=b'/\cos\theta+a-f$ increases by less than 1% as θ increases from 0 to 10 deg. Thus, by

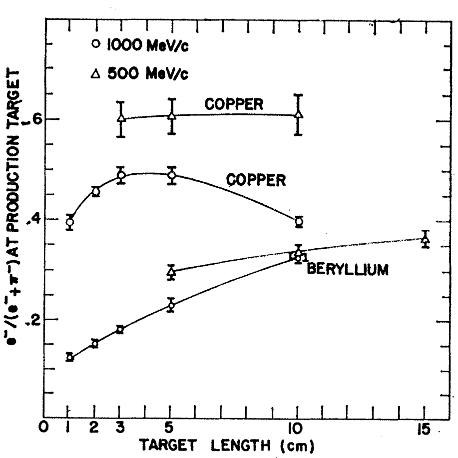

FIG. 11. Ratio of electrons to fast negative particles at the production target.

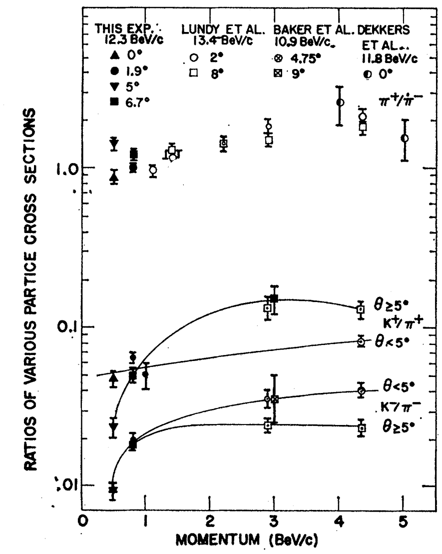

FIG. 12. Comparison of cross section ratios from beryllium with data from other experiments.

assuming $(b+a-f)$ to have the same value for 0, 5, and 10 deg production, a least-squares fit was applied to the set of simultaneous equations

$$Y(L,\theta)=(\rho N_0 L/A)\sigma_0(\theta)e^{-(b+a-f)L/2}$$

with $\theta=0$, 5, and 10 deg. This yielded the values of the four unknown parameters $\sigma_0(0)$, $\sigma_0(5)$, $\sigma_0(10)$, and $(b+a-f)$.

Multiple scattering of secondary particles in the target was investigated by a Monte Carlo technique and also by application of Sternheimer's analysis of multiple scattering corrections for counter experiments.[5] The result in either case is that particles scattered out of the

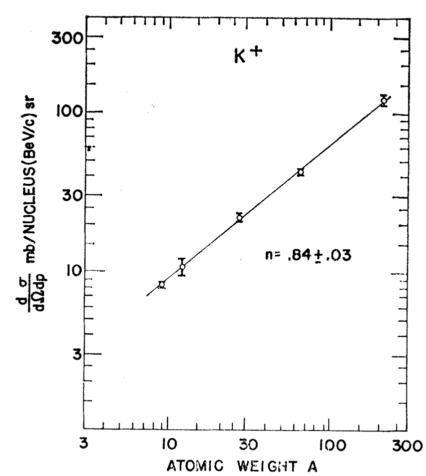

FIG. 13. Differential production cross sections of 820-MeV/c K^+ at 0° from a variety of target materials.

[5] R. M. Sternheimer, Rev. Sci. Instr. 25, 1070 (1954).

TABLE V. Exponential dependence of production cross sections on atomic weight ($\sigma \propto A^n$).

Particle	n
π^+	0.68 ± 0.02
π^-	0.66 ± 0.02
K^+	0.84 ± 0.03
K^-	0.78 ± 0.04
p	1.02 ± 0.03

angular acceptance of the beam are compensated by those scattered in to better than 2%. This is in agreement with the observations of Jordan.[6] Tertiary particle production was also estimated and found to be small.

IV. RESULTS

All of the differential production cross sections are listed in Tables II and III. In addition, the beryllium data are presented graphically in Figs. 6–10. For convenience, the angles are labeled 0, 5, and 10 deg. The actual measured values of the production angles for each momentum are given in Table IV.

The production cross section of He^{4++} is less than 2% of the deuteron cross section. This was determined by taking a range curve, since both particles appear in the same peak of the time-of-flight spectrum.

The cross sections are given in mb per nucleus (BeV/c) sr. The errors quoted for the cross sections include the statistical errors (standard deviations) and estimated systematic uncertainties. The lines connecting the data points are merely to guide the eye.

Electron contaminations at the production target for copper and beryllium at 500 MeV/c and 1000 MeV/c are plotted in Fig. 11.

The least-squares fit of the yield data resulted in an average χ^2 per deg of freedom of 0.55 for typically 3 deg of freedom. The fitted values of $(b+a-f)$ agreed well with the values calculated from known absorption cross sections.

A comparison between the ratios K^+/π^+, K^-/π^-, and π^+/π^- from this experiment and from others[7–9] in the same incident proton momentum range is shown in Fig. 12.

Figure 13 displays 820 MeV/c K^+ cross sections as a function of the atomic weight of the target material A. Target materials investigated in addition to copper and beryllium were carbon, aluminum, and lead. A least-squares fit of the data to the functional form A^n gives slightly differing values of n for the various particles, as shown in Table V.

V. CONCLUSIONS

It is evident from the data that the differential production cross sections for the various particles peak in the neighborhood of 5–10 deg although the enhancement relative to zero deg production is not large $[1\leq\sigma(\theta)/\sigma(0°)<2]$. Other experiments have shown that at fixed production angle, the cross sections peak in the vicinity of 1–3 BeV/c.[7–9] Our data indicate that the cross sections do indeed begin to level off near 1 BeV/c.[10]

It was found that electron contaminations in low-momentum beams are large. The fraction of electrons at the production target exceeds 40% for copper and 20% for beryllium targets of reasonable lengths (1–10 cm). Thus, whenever feasible, beryllium is preferable to copper as a source for low-momentum pion beams.

ACKNOWLEDGMENTS

We would like to thank D. A. Burandt, E. R. Hayes, J. S. Upton, J. O. Tate, and J. Terandy for their help. We are grateful to the personnel of the Particle Accelerator Division and the Experimental Planning and Operations Group for their support during this experiment. We would also like to express our appreciation for the assistance rendered by A. F. Stehney, E. P. Steinberg, and personnel of the Argonne High Energy Nuclear Chemistry Group in the gold foil-activation measurements.

[6] B. Jordan, CERN Report No. 65-14, 1965 (unpublished).

[7] D. Dekkers, J. A. Geibel, R. Mermod, G. Weber, T. R. Willitts, K. Winter, B. Jordan, M. Vivargent, N. M. King, and E. J. Wilson, Phys. Rev. **137**, B962 (1965).

[8] W. F. Baker, R. L. Cool, E. W. Jenkins, T. F. Kycia, S. S. Lindenbaum, W. A. Love, D. Luers, J. A. Niederer, S. Ozaki, A. L. Read, J. J. Russell, and L. C. L. Yuan, Phys. Rev. Letters **7**, 101 (1961).

[9] R. A. Lundy, T. B. Novey, D. D. Yovanovitch, and V. L. Telegdi, Phys. Rev. Letters **14**, 504 (1965); **14**, 730(E) (1965).

[10] Sanford and Wang have developed an eight-parameter semi-empirical formula which reproduces well the beryllium production data of many experiments. The variables of the formula are the incident proton momentum, the secondary particle momentum, and production angle. The inclusion of the results of this experiment in the least-squares fit slightly improves the agreement of the formula with all the data. J. R. Sanford and C. L. Wang, AGS Internal Report No. JRS/CLW-1, 1967 (unpublished); and AGS Internal Report No. JRS/CLW-2, 1967 (unpublished).